Vision Research 51 (2011) 2186–2197

Contents lists available at SciVerse ScienceDirect

Vision Research

journal homepage: www.elsevier.com/locate/visres

The role of transparency in da Vinci stereopsis

Marina Zannoli *, Pascal Mamassian

Laboratoire Psychologie de la Perception (CNRS UMR 8158), Université Paris Descartes, France

ARTICLE INFO

Article history:
Received 7 February 2011
Received in revised form 12 August 2011
Available online 28 August 2011

Keywords:
da Vinci stereopsis
Half occlusion
Perceptual transparency
Binocular models

ABSTRACT

The majority of natural scenes contains zones that are visible to one eye only. Past studies have shown that these monocular regions can be seen at a precise depth even though there are no binocular disparities that uniquely constrain their locations in depth. In the so-called da Vinci stereopsis configuration, the monocular region is a vertical line placed next to a binocular rectangular occluder. The opacity of the occluder has been mentioned to be a necessary condition to obtain da Vinci stereopsis. However, this opacity constraint has never been empirically tested. In the present study, we tested whether da Vinci stereopsis and perceptual transparency can interact using a classical da Vinci configuration in which the opacity of the occluder varied. We used two different monocular objects: a line and a disk. We found no effect of the opacity of the occluder on the perceived depth of the monocular object. A careful analysis of the distribution of perceived depth revealed that the monocular object was perceived at a depth that increased with the distance between the object and the occluder. The analysis of the skewness of the distributions was not consistent with a double fusion explanation, favoring an implication of occlusion geometry in da Vinci stereopsis. A simple model that includes the geometry of the scene could account for the results. In summary, the mechanism responsible to locate monocular regions in depth is not sensitive to the material properties of objects, suggesting that da Vinci stereopsis is solved at relatively early stages of disparity processing.

1. Introduction

There is more to binocular vision than the matching of corresponding objects in the left and right images. Since the early physiological recordings of Hubel and Wiesel in cats (1959), binocular disparity was thought to be processed in area V1 and extrastriate areas (MT in primates) primarily (Howard & Rogers, 2002; Parker, 2007). Within the last decade this classical view has been challenged by several studies in electrophysiology and imaging indicating that disparity processing might be distributed across several regions of the visual cortex (Backus et al., 2001). For example, Preston et al. (2008) showed that areas V3 and V4 are sensitive to both correlated and anticorrelated stimuli. These results suggest that there exist many steps of processing between the extraction of the disparity signal to the computation of the depth map. One of them consists in determining depth ordering relationships between objects, namely which object is in front of another without any precise estimate of the distance between the two. Traditionally, depth ordering has been associated with monocular cues based on luminance such as transparency (Anderson, 2008) or occlusion (Sekuler & Palmer, 1992). Yet, binocular cues can be equally efficient in conveying depth ordering information. In particular, da Vinci stereopsis provides a convincing illustration of the interaction between occlusion and stereopsis.

1.1. da Vinci stereopsis and occlusion geometry

In 1508, Leonardo da Vinci noticed that next to a vertical edge of an opaque object is a region of a far surface that is visible to only one eye (see Fig. 1). Boundaries of objects produce a lot of depth discontinuities. These abrupt changes in depth can create a number of points that are present in one retinal image only. One can assume that the visual system automatically ignores these monocular points to solve the correspondence problem. However, a majority of these unpaired points present in natural visual scenes carry crucial information about depth relationships between objects (see Harris and Wilcox (2009) for a comprehensive review). The first study on the role of half-occlusions, conducted by Lawson and Gulick (1967), demonstrated that occlusion cues can signal a depth offset. Later, Gillam and Borsting (1988) used random-dot stereograms and added half-occlusion regions that could be either congruent or incongruent with the disparity information. They showed that observers were faster to detect a depth edge in the congruent condition than in the incongruent case. Two types of configurations can lead to the presence of monocular regions: occlusion and camouflage (see Fig. 1a).

* Corresponding author.
E-mail address: marinazannoli@gmail.com (M. Zannoli).

0042-6989/$ - see front matter © 2011 Elsevier Ltd. All rights reserved.
doi:10.1016/j.visres.2011.08.014

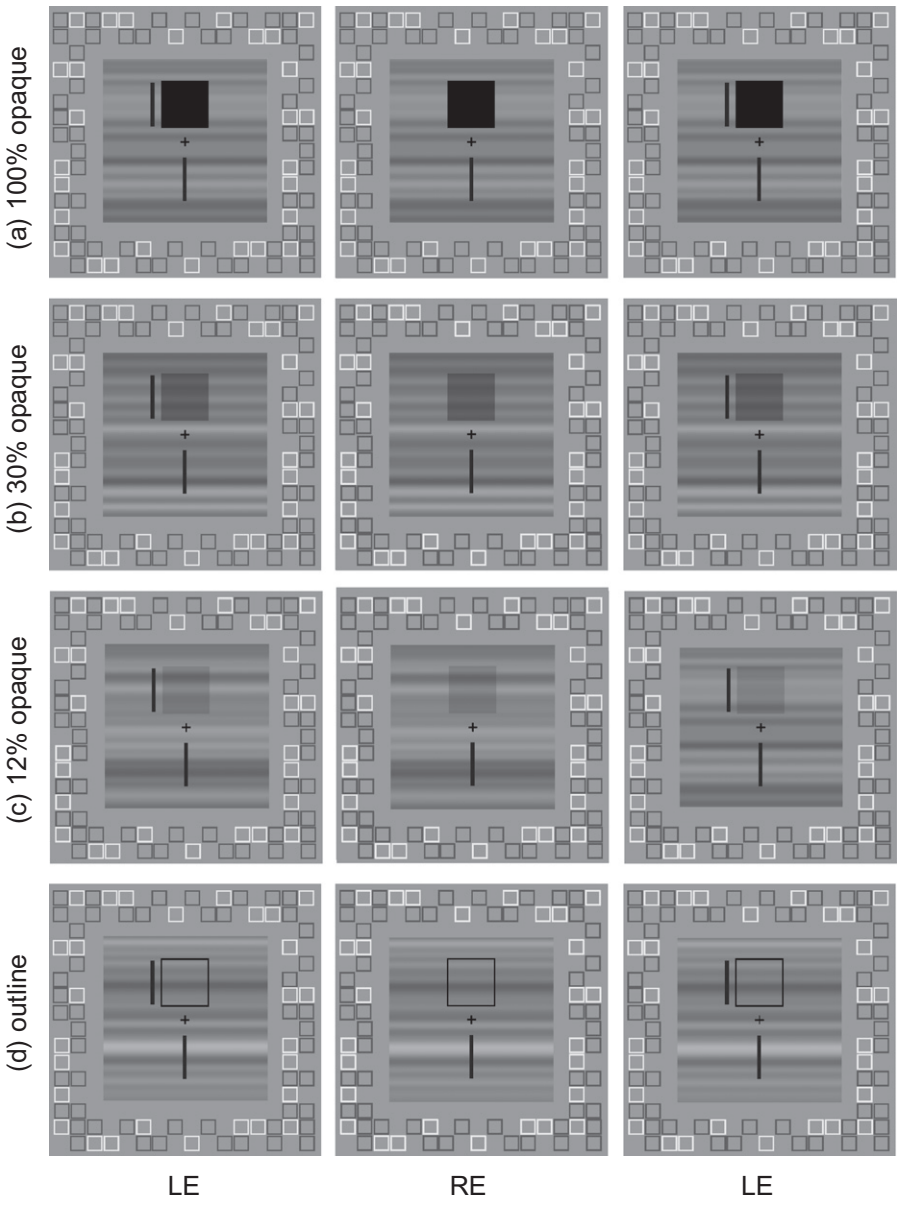

Fig. 1. Stimulus used in Experiment 1. The valid condition can be seen by parallel-fusing the first and second columns. The invalid condition is seen when parallel-fusing the second and third columns. (a) Classical da Vinci configuration where the occluder is completely opaque. (b) Condition where the occluder is 30% opaque. (c) Condition where the occluder is 12% opaque. (d) Condition where the occluder is just represented by its outline.

On the basis of da Vinci's drawings, Nakayama and Shimojo (1990) used a simple stimulus configuration where a monocular vertical line is presented close to a binocular rectangle to investigate the role of the stimulus geometry and ecological validity on the perceived depth of monocular points (see Fig. 1). In this half-occlusion configuration, the rectangle acts as an occluder. When the line was presented on the temporal side of the occluder (in an ecologically "valid" configuration), the authors found that the line was perceived at a precise depth that depended on the line-occluder distance (or line eccentricity). They called this impression of depth "da Vinci stereopsis". On the contrary, when presented to the nasal side ("invalid" condition), the line was perceived at the depth of the occluder (see Fig. 2 for detailed predictions). To explain these results, the authors postulated that the visual system is able to extract the geometry of the scene and the occlusion relations in it. Then, the position of the monocular objects, the eye-of-origin information and the geometry are combined to compute the perceived depth of the unpaired points. The edges of the occluder define constraint lines delimitating a constraint zone. This constraint zone hidden to one eye defines the area in which a monocular object must lie to refer to an ecologically valid situation. The perceived depth increases with eccentricity and corresponds to the minimal possible depth, defined by the nearest constraint line (Nakayama & Shimojo, 1990). Beyond an eccentricity of 30–40 arcmin, the line regresses to the occluder depth (Nakayama & Shimojo, 1990). Nakayama and Shimojo's "invalid condition" is obtained by switching the two eye's views from the "valid condition". In this case, if the monocular object has the same texture and luminance as the foreground, it is "camouflaged" in one eye (and therefore invisible) and not in the other. Interestingly, the visual system does not seem to treat occlusion and camouflage equally, considering camouflage as very unlikely (but see Cook and Gillam (2004) for a case in which camouflage was easier than occlusion).

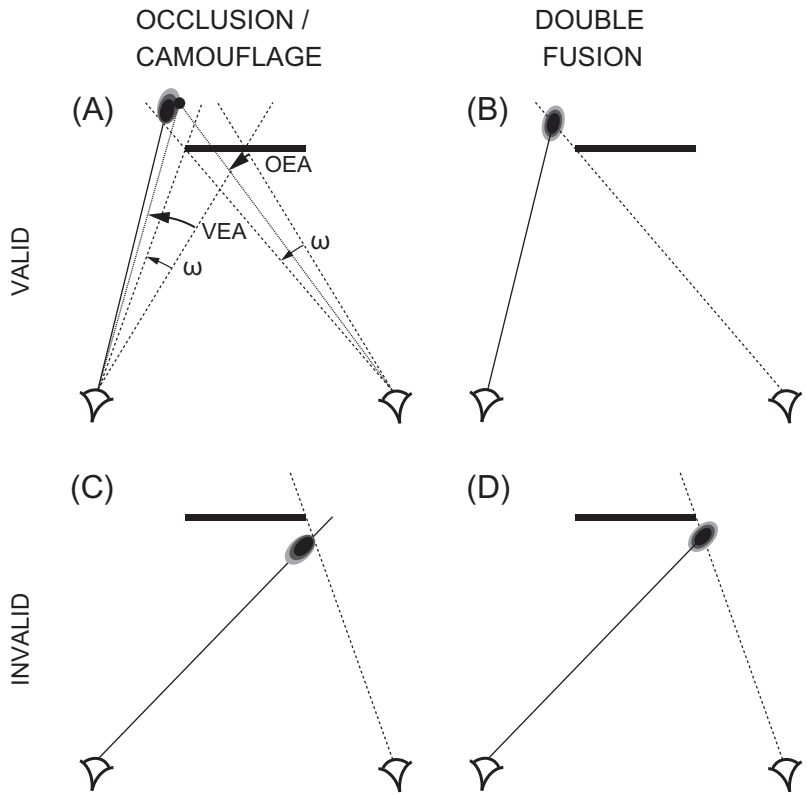

Fig. 2. Definitions of angles and predictions of the occlusion/camouflage and double fusion hypotheses. By convention, the monocular object is always presented to the left eye. (a) Definitions: the dot is an example of the location of the perceived monocular object for one trial, the *Other Eye Angle* (OEA) is its perceived depth for that trial and the *Viewing Eye Angle* (VEA) is its perceived azimuth. The ω angle represents half of the occluder's width. This figure also shows the predictions for the valid condition under the occlusion scenario: the predicted shape of the distribution of percepts is illustrated by contour plots (darker is more likely). (b–d) Predictions for the valid/double fusion case, the invalid/occlusion case and the invalid/double fusion case respectively.

1.2. Da Vinci stereopsis and double fusion

A few years later, several authors pointed out the similarity between the configuration used by Nakayama and Shimojo and Panum's limiting case. When two vertical lines presented to one eye are fused with a single line presented to the other eye, they are perceived as two lines in depth (Panum, 1858). This depth effect can be explained by a double fusion process in which the single line is fused separately with each of the two lines in the other image (Gillam, Blackburn, & Cook, 1995). The resulting depth depends on the disparity between the two lines.

Due to similarities between the two configurations, some authors have tried to find a common explanation, supposing that one is a simple variation of the other. Ono, Shimono, and Shibuta (1992) reported results similar to Nakayama and Shimojo's findings with a Panum's limiting case stimulus and hypothesized that it is a special case of da Vinci stereopsis. Gillam, Blackburn, and Cook (1995) used a stimulus similar to Ono, Shimono, and Shibuta (1992) and obtained results favoring a double fusion explanation for both Panum's limiting case and da Vinci stereopsis. In the latter case, the monocular line would be "double-fused" with the adjacent edge of the occluder in the other eye. The line would be seen in front or behind the occluder depending on the eye to which the line is presented (see Fig. 2 for detailed predictions). Later, Gillam, Cook, and Blackburn (2003) designed a da Vinci stimulus in which the monocular object is a disk that cannot be "double-fused" with the adjacent edge of the occluder. They found that the perceived depth was qualitative but not quantitative in the sense that it only signaled depth ordering. They also reported that this perceived depth depended on the validity of the scene configuration, suggesting a double fusion explanation for da Vinci stereopsis.

1.3. Aims of the study

The main aim of the present study was to investigate the importance of opacity on da Vinci stereopsis using perceptual transparency (Metelli, 1985; Singh & Anderson, 2002). If the degree of transmittance of the occluder influences the perceived depth in da Vinci stereopsis, this suggests that sophisticated aspects of the scene are taken into account during construction of the depth map as suggested by Nakayama and Shimojo. In contrast, if the processing of monocular regions does not depend on the opacity of the occluder, then low-level binocular mechanisms, such as double fusion, might be sufficient to explain da Vinci stereopsis. A secondary aim of the study was to estimate the consistency of the depth reports in da Vinci configurations. This consistency was measured by recording the whole distribution of depth percepts and by analyzing the spread and other statistical aspects of this distribution.

2. Experiment 1

To test whether da Vinci stereopsis is sensitive to the material properties of occluding objects, we manipulated perceptual transparency. According to the model of Singh and Anderson (2002), the opacity of a transparent surface is determined by the contrast ratio of the lower contrast regions (region of transparency) relative to the higher contrast regions (background) (see Fig. 1). We consider that this type of transparency has several advantages. First, the degree of opacity can be manipulated extremely precisely, allowing us to test whether opacity is fully required and whether it has a quantitative effect on da Vinci stereopsis. Psychophysical and neurophysiological studies suggest that the computation needed

to extract the transmittance (and thus the depth ordering) requires an intermediate level of processing (Qiu & von der Heydt, 2007; Singh & Anderson, 2002). Perceptual transparency thus represents a complex depth cue. Using such a mid-level cue allows us to assess the level of processing required to compute the occlusion geometry in da Vinci stereopsis.

2.1. Methods

2.1.1. Participants

Four naïve observers with normal or corrected-to-normal vision were recruited in the laboratory building. All participants had experience in psychophysical observation and had normal stereo acuity and transparency sensitivity.

2.1.2. Stimulus presentation

The stereograms were presented on a CRT monitor (ViewSonic 21″, resolution of 1280 × 960, refresh rate of 85.0 Hz) using a modified Wheatstone stereoscope at a simulated distance of 1 m. Each eye viewed one horizontal half of the CRT screen. A chin rest was used to stabilize the observer's head and to control the viewing distance. The monitor was linearized in luminance (gamma corrected). The display was the only source of light and the stereoscope was calibrated geometrically to account for each participant's interocular distance.

2.1.3. Stimuli

Stimuli were generated using the Psychophysics Toolbox (Brainard, 1997; Pelli, 1997). A binocular black (5 cd/m^2) square was presented in the upper visual field (1.3° from the center). We denote by ω the half width of the occluder: $\omega = 0.8°$. A monocular black line of 0.1×1.6 deg^2 was presented next to the square. Another black line of 0.1×1.6 deg^2 was presented binocularly in the lower visual field. These three elements were presented on a textured background. The background was a 1-dimensional noise texture produced by blurring a texture of random 1-pixel-wide horizontal stripes with a vertical Gaussian (SD 1.15°). The background was comparable to a wallpaper stimulus, in the sense that there was a complete ambiguity on correspondence (see Fig. 1). The degree of opacity of the black square varied randomly between three values (100%, 30% and 12% opaque) chosen on the basis of pilot experiments. The transparent square was defined by changing the alpha index (Brainard, 1997; Pelli, 1997; Porter & Duff, 1984) of the binocular square region of the background area. An "outline" condition in which the binocular square was only defined by its edges (thickness of 0.03°) was added.

The distance between the monocular line and the black square varied randomly between three values. We denote by ε the eccentricity between the monocular line and the closest edge of the occluder. Three values were chosen for ε: 10, 19 and 28 arcmin. These values were chosen to match Nakayama and Shimojo's (1990) stimulus configurations. The eye of presentation (left or right) of the monocular line was counterbalanced and the side of presentation (left or right of the square) varied randomly to create four different conditions. In the "valid" condition, the line was presented to the temporal side of the square and in the "invalid" condition the line was presented to the nasal side (see Fig. 2).

The textured background was surrounded by a vergence-stabilization frame consisting of multiple black and white small squares (0.35×0.35 deg^2; black: 5 cd/m^2 and white: 80 cd/m^2) presented on a gray background (55 cd/m^2). Black nonius lines were added at the center.

2.1.4. Procedure

While keeping the nonius lines aligned, participants were asked to evaluate the perceived azimuth and depth positions of the monocular line using an adjustment procedure. The observers controlled the horizontal position and depth coordinates of the stereo-probe located in the lower visual field using the four keyboard directional arrows: the left and right arrows controlled for the azimuth position of the stereo-probe while the up and down arrow keys controlled for the depth. The stereo-probe appeared at the central position at the beginning of each trial. The impression of depth was created by adding positive or negative disparity to the lines between the two eyes' images. The participants were instructed to privilege accuracy rather than speed. Final spatial coordinates of the stereo-probe were recorded separately for the right and left image for each trial. Each combination of eccentricity values, eye-of-origin, opacity values and validity configurations was repeated 12 times in total. The experiment was divided in four sessions.

2.1.5. Data analysis

We define two visual angles to analyze the results. The *Viewing Eye Angle* (VEA) is the angle between the center of the occluder and the position of the probe for the eye that sees the monocular line. It gives an estimation of the horizontal position of the probe (*i.e.* the perceived azimuth of the monocular line – Fig. 2a). The *Other Eye Angle* (OEA) is the angle between the center of the occluder and the position of the probe for the eye that *does not* see the monocular line. It gives an estimation of the depth position of the probe (*i.e.* the perceived depth of the monocular line – Fig. 2a).

Data were pooled across the "side of the line" factor to bring the total number of trials per condition to 24.

2.1.6. Predictions

Different predictions can be advanced depending on the underlying explanations of da Vinci stereopsis.

2.1.6.1. Occlusion/camouflage hypothesis. If we follow strictly the occlusion geometry we predict that, in the valid condition, the monocular line should be occluded to the other eye and thus be perceived inside the far monocular zone (OEA < ω; see Fig. 2a). In the invalid condition, we predict that the monocular line would be camouflaged by the occluder to the other eye and therefore be perceived into the near monocular zone (*i.e.* again OEA < ω).

Extrapolating Nakayama and Shimojo's findings (1990), we can make slightly different predictions. We expect that the monocular line would be perceived on the near edge of the monocular zone (*i.e.* at the minimum possible depth: OEA $\approx \omega$) in the valid condition. In the invalid condition, we expect that the monocular line will be perceived at the depth of the occlusion plane (in this case, the fixation plane: OEA $\approx \omega + \varepsilon$).

If da Vinci stereopsis relies on occlusion characteristics, we expect an effect of the opacity of the occluder on the perceived depth of the monocular line. More precisely, the impression of depth should decay as the occluder gets more transparent. In the extreme outline condition, perceived depth should be consistent with double fusion.

Regarding the perceived position of the line for the viewing eye, we naturally predict that its location should be veridical in both "valid" and "invalid" conditions (VEA $\approx \omega + \varepsilon$; see Fig. 2a and c).

2.1.6.2. Double fusion hypothesis. According to the double fusion hypothesis, the distance between the monocular line and one edge of the occluder is processed as disparity. In this case, the line is seen in front or behind the occluder depending on the "validity" variable. This variable determines the sign of the disparity value. Following the double fusion hypothesis, we therefore expect that the monocular line would be perceived at the intersection of the line of sight going from the viewing eye to the monocular line and the line of sight going from the other eye to the adjacent edge of the occluder. Therefore, we expect the OEA and VEA coordinates

to be the same in both validity conditions (OEA $\approx \omega$ and VEA $\approx \omega + \varepsilon$; see Fig. 2b and d).

If da Vinci stereopsis is based on double fusion, we expect the opacity of the occluder to have no effect on the perceived depth of the monocular line.

2.1.6.3. Disentangling between occlusion and double-fusion. To sum up, occlusion and double fusion hypotheses give roughly the same predictions even though they rely on different underlying mechanisms. To disentangle the two explanations, we introduce a novel analysis using the shape of the distributions of depth estimations. In the double fusion hypothesis, OEA is treated as a disparity value whereas it represents a constraint line in the occlusion hypothesis. To account for this, we postulate that the distributions of perceived depths should be symmetrically distributed around the predicted value in the double fusion case: the uncertainty is equivalent in all depth directions. In contrast, in the occlusion case, we expect the distributions of perceived depths to be skewed to account for the constraints that define the monocular zones: the monocular line can be seen anywhere in the monocular zone but not outside this area (see Fig. 2a).

If surface material plays a role in da Vinci stereopsis, we expect a change in the skewness of the distributions of perceived depth with transparency in the occlusion case. A more opaque surface could more easily hide an object to the other eye, so there should be more skewness with more opacity.

2.2. Results

We treat the outline condition as a 0% opacity condition. Because no significant difference was found between the side of presentation conditions (left or right), OEA and VEA values were pooled across this factor and all results are presented as if they resulted from the left eye condition. When the monocular line is viewed by the left eye, it is presented on the left side of the occluder in the valid condition and on the right side in the invalid condition. The distributions of OEA and VEA reports are shown in Figs. 3 and 4.

2.2.1. Main effects of experimental variables

The OEA (depth) and VEA (azimuth) distributions were very consistent across subjects. Before conducting inferential analyses, we tested the normality of the OEA and VEA distributions obtained for each (eccentricity $*$ validity $*$ opacity) condition using the D'Agostino's normality test (D'Agostino, Belanger, & D'Agostino, 1990). Except for one VEA distribution ($\varepsilon = 19$ in the valid condition), all distributions were non-normal ($X2$ values ranging from 19.1 to 159). To take into account this non-normality, a repeated measures Analysis of Variance was conducted on the medians (and not the mean) for each validity condition separately. The ANOVA conducted on the OEA measures revealed a significant effect of eccentricity ($F(2,6) = 405$, $P < 0.001$ for the valid condition and $F(2,6) = 170$, $P < 0.001$ for the invalid condition) but no effect of opacity ($F(3,9) = 0.573$, $P = 0.647$ for the valid condition and $F(3,9) = 2.87$, $P = 0.096$ for the invalid condition – see Fig. 3). The ANOVA conducted on the VEA measures revealed the same pattern of results (eccentricity: $F(2,6) = 150$, $P < 0.001$ for the valid condition and $F(2,6) = 545$, $P < 0.001$ for the invalid condition; opacity: $F(3,9) = 3.24$, $P = 0.075$ for the valid condition and $F(3,9) = 0.426$, $P = 0.739$ for the invalid condition – see Fig. 3).

Because no effect of transparency was found, data were averaged across all opacity conditions for further analyses (see Figs. 4 and 5). Confidence intervals for the medians were computed using bootstrapping (Efron & Tibshirani, 1994) for each (eccentricity $*$ validity) condition for both OEA and VEA values.

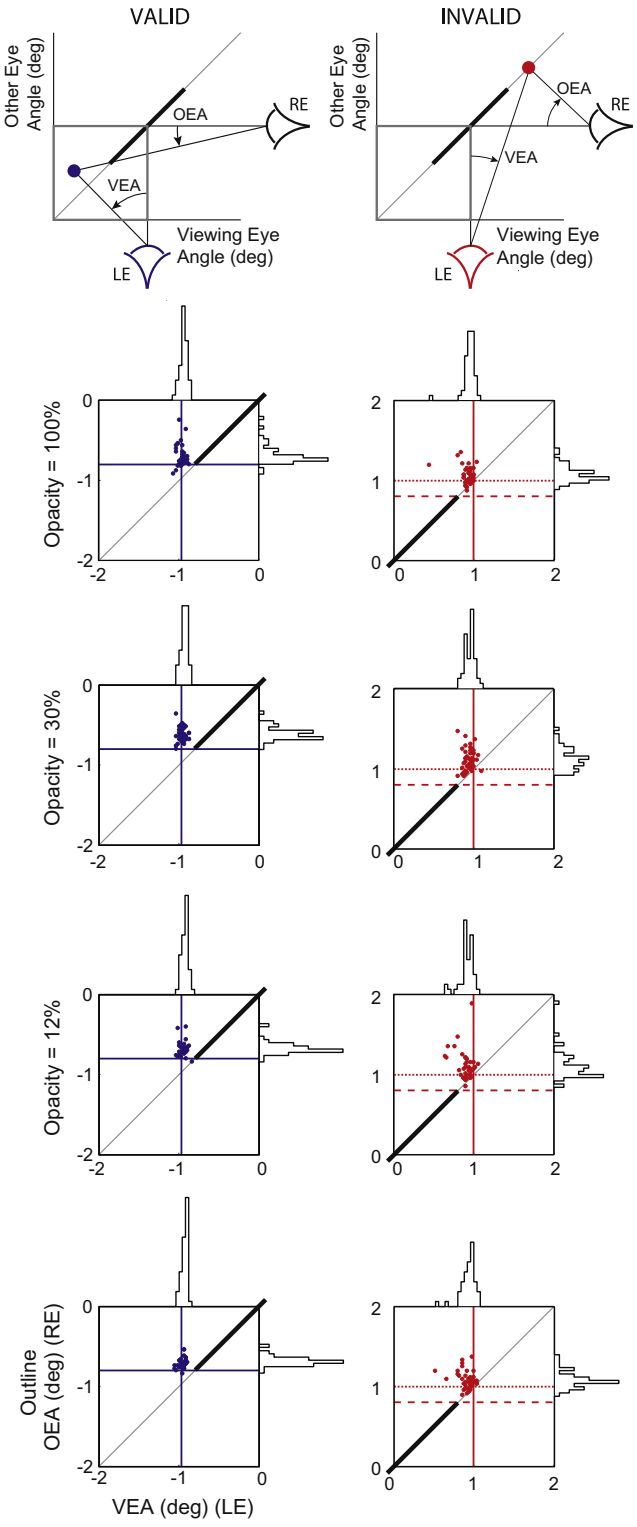

Fig. 3. Results of Experiment 1 for the opacity variable. The valid conditions (in blue) are shown in the left column and the invalid conditions (in red) in the right column. The top row illustrates the format used to plot the relationship between Viewing Eye Angle (VEA) and Other Eye Angle (OEA). The next four rows display the data for each of the four opacity conditions for the 10 arcmin eccentricity condition. Each colored dot is one percept reported by one observer. Data are pooled across all side conditions (all figures are plotted as if the monocular line were seen by the left eye). The gray diagonal line represents the zero disparity plane. The thick black line represents the position of the occluder and the colored lines show the monocular object lines of sight for both eyes and the predictions (the dotted and dashed lines represent the occlusion and double fusion predictions for the OEA respectively). The intersections of the colored lines show the different hypotheses predictions.

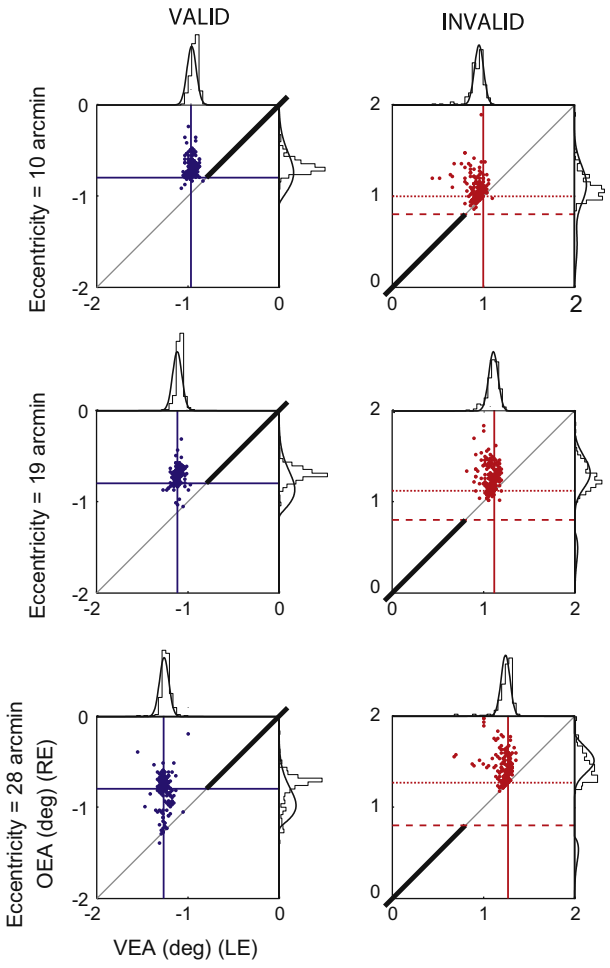

Fig. 4. Results of Experiment 1. Data are pooled across all transparency and side conditions. The three rows display the data for each of the three eccentricities of the monocular line. See legend from Fig. 3 for details.

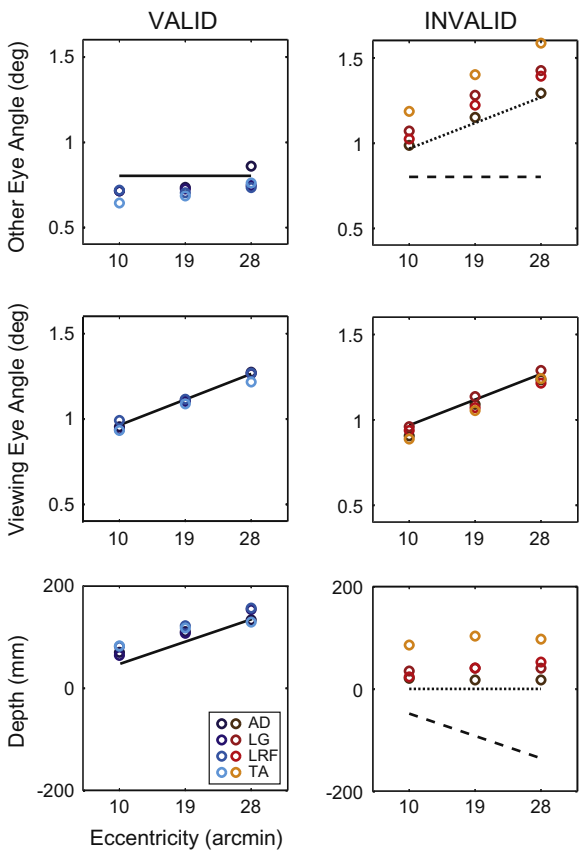

Fig. 5. Individual medians for Experiment 1. Data are averaged across all transparency and side conditions. Predictions are plotted as horizontal lines. Dashed lines represent double fusion predictions while dotted lines show occlusion predictions. Solid lines indicate same predictions for double fusion and occlusion hypotheses. Top row: Absolute values for median OEA (depth) estimations and predictions. Middle row: Absolute values for median VEA (azimuth) estimations and predictions. Bottom row: Median depth estimations in mm with and predictions. Data in blue show median estimations in the valid condition while data in red show median estimations in the invalid condition. Different shades of blue and orange represent different observers.

2.2.1.1. Valid condition. In the valid condition, the OEA values were significantly smaller than the occlusion/double fusion predictions (ω) for the three eccentricities (CI for ε_{10}: [0.684 0.723], CI for ε_{19}: [0.709 0.723], CI for ε_{28}: [0.739 0.777], prediction = 0.8). In other words, when consistent with the geometry of the scene, the line was perceived in the constraint zone. The VEA values were not different from occlusion and double fusion predictions ($\omega + \varepsilon$) for the three eccentricities (CI for ε_{10}: [0.942 0.964], prediction = 0.967; CI for ε_{19}: [1.08 1.12], prediction = 1.12; CI for ε_{28}: [1.24 1.28], prediction = 1.27), meaning that the line was perceived at the position predicted by the monocular object line of sight.

2.2.1.2. Invalid condition. The OEA values were significantly larger than the occlusion predictions ($\omega + \varepsilon$) for the three eccentricities (CI for ε_{10}: [1.033 1.080], prediction = 0.967; CI for ε_{19}: [1.22 1.27], prediction = 1.12; CI for ε_{28}: [1.38 1.44], prediction = 1.27), indicating that the monocular line was perceived behind the occluder plane. The distance between these depth estimations and the predictions tended to increase with eccentricity. The VEA values were significantly smaller than the value predicted by occlusion and double fusion ($\omega + \varepsilon$) for the 10 and 19 arcmin eccentricities (CI for ε_{10}: [0.922 0.948], prediction = 0.967; CI for ε_{19}: [1.08 1.10], prediction = 1.12) and not different from this prediction for the largest eccentricity (CI for ε_{28}: [1.23 1.27], prediction = 1.27).

2.2.2. Skewness

2.2.2.1. Other Eye Angle. In the valid condition for the 10 and 19 arcmin conditions, we observe a positive skewness (mean skewness for 10 arcmin condition = 0.726; mean skewness for 19 arcmin condition = 0.267). For the largest eccentricity we observe a negative skewness for the four observers (mean skewness for 28 arcmin condition = −0.706). In the invalid condition, the skewness of the OEA distribution is positive for all three eccentricities for the four observers (mean skewness for 10 arcmin condition = −0.894; mean skewness for 19 arcmin condition = 0.773 and mean skewness for 28 arcmin condition = 0.620).

2.2.2.2. Viewing Eye Angle. In the valid condition, the skewness of VEA distributions is very small and positive on average (mean skewness for 10 arcmin condition = 0.076; mean skewness for 19 arcmin condition = 0.152 and mean skewness for 28 arcmin condition = 0.093). The sign of this skewness means that the monocular line was perceived slightly biased toward the position of the occluder. In the invalid condition, the skewness of VEA distributions is again small but negative on average (mean skewness for 10 arcmin condition = −0.427; mean skewness for 19 arcmin condition = −0.100 and mean skewness for 28 arcmin condition = −0.401). Symmetrically, the sign of this skewness means that the monocular line was perceived slightly biased toward the position of the occluder.

2.3. Discussion of Experiment 1

2.3.1. Summary of results

The 100% opaque condition served as a classical da Vinci stereopsis baseline condition. The method of adjustment we used allowed us to collect precise estimations of the perceived line position. No effect of the opacity of the occluder was found on the perceived depth of the monocular line. For all conditions, the distribution of values for the VEA (Viewing Eye Angle, corresponding to the perceived azimuth of the monocular line) was narrowly peaked around the point predicted by the line of sight constraint but slightly asymmetric, indicating that the line was perceived slightly deviated towards the position of the occluder. On the contrary, the distribution of values for the OEA (Other Eye Angle, corresponding to the perceived depth of the monocular line) was widespread and skewed toward uncrossed disparities for the low validity conditions.

Contrary to our predictions, we found a significant effect of eccentricity in the valid condition for the OEA distribution. However, as shown in Fig. 4, this effect is small and median estimations follow predictions very closely. This effect can be attributed to a regression phenomenon previously reported by several authors (Häkkinen & Nyman, 1996; Nakayama & Shimojo, 1990). We discuss this regression in the light of a simple model in a later section.

2.3.2. No effect of transparency

All observers reported a vivid sensation of transparency and were sensitive to changes in the transmittance of the occluder. Therefore, we can assume that the opacity of the occluder was efficiently varied across the different opacity conditions.

Even though it is hazardous to assert anything from negative results, our attempts to find an effect of transparency on da Vinci stereopsis have failed. According to Nakayama and Shimojo (1990), the visual system extracts the occlusion geometry of the scene by detecting unpaired features, eye-of-origin information, depth discontinuities, object edges and opacity relationships. This geometry of occlusion is then used to determine the spatial location of these unpaired features. The experimental paradigm used by Nakayama and Shimojo (1990) did not allow them to test if da Vinci stereopsis is processed during the matching step or if the depth of the monocular object is determined once a satisfying solution to the correspondence problem has been found. These authors made no assertions about the level of processing required to compute this geometry. Our results thus suggest two alternative hypotheses. Either da Vinci stereopsis is solved before perceptual transparency is solved, or the geometry of occlusion does not include opacity information.

2.3.3. Skewness

Previous studies on da Vinci stereopsis did not dwell on the distributions of perceived depth estimations. However, the particular shape of such distributions is instructive with respect to the occlusion and double fusion hypotheses.

According to the occlusion hypothesis, an asymmetry could be expected for the OEA values in the valid condition (see Fig. 2a). In this condition, the depth estimation is constrained on one side by the minimal depth defined by the adjacent occluder's edge. In other words, this constraint forbids depth estimates that would make the line visible by both eyes, but is oblivious about depth estimates that place the line behind the occluder. The particular type of skewness we found for the OEA values in the valid condition are exactly consistent with this idea: in the 10 and 19 arcmin conditions, the distribution of OEA values had a positive skewness, extending into the occluder region. For the largest eccentricity, the mean skewness was in the other direction (negative). This spread can be explained by a phenomenon of regression to the occluder's plane (a similar interpretation was proposed by Nakayama and Shimojo (1990) and Häkkinen and Nyman (1996)). In the invalid condition, the occlusion hypothesis as stated by Nakayama and Shimojo's (1990) does not make a clear prediction with respect to the skewness of the distribution of perceived depths.

According to the double fusion hypothesis, the monocular line has a clear correspondence in the other eye (the edge of the occluder). The uncertainty in matching the monocular line with the edge should be symmetrical if matching is based on image intensity changes. However, one might argue that this uncertainty could be asymmetrical given that the monocular line can be matched with any part of the occluder. In all cases, we do not expect any change of skewness with eccentricity, or between the valid and the invalid conditions. The fact that skewness was significant in the observers' data, and that it changed across conditions, cannot be easily explained by the double fusion hypothesis.

2.3.4. Occlusion vs. double fusion

There has been an intense debate about a double fusion explanation for the phenomenon of da Vinci stereopsis (Gillam, Cook, & Blackburn, 2003; Ono et al., 1992; Pianta & Gillam, 2003). We now review how the occlusion and the double fusion hypotheses can explain our results.

Predictions following double fusion are straightforward. In both valid and invalid conditions, the perceived depth of the monocular line is computed using the distance to the occluder as disparity. If presented to the temporal side of the occluder, this disparity is uncrossed and the line is perceived further away than the occluder. Reciprocally, the line is perceived in front of the occluder when presented to the nasal side.

Predictions following the occlusion hypothesis are more complex. In the valid condition, the monocular object should be perceived behind the occluder, and therefore at a depth at least equal to the minimal depth predicted by the geometry. In the invalid condition, there is room for a symmetric interpretation where the monocular object is camouflaged by the large binocular object. However, Nakayama and Shimojo (1990) preferred the interpretation that the visual system is unable to find an adequate solution to it and thus places the monocular object at the same depth as the occluder.

Our data are more consistent with the occlusion than with the double fusion hypothesis. In the invalid condition, none of our observers perceived the monocular object in front of the occluder plane. In addition, in the valid condition, the monocular line was perceived at a depth significantly larger than the minimal depth predicted by the three eccentricities. Together with the discussion in the section above on the skewness of the distributions of perceived depths, our data therefore appear inconsistent with the double fusion hypothesis. With respect to the occlusion hypothesis, our data clearly follow the predictions in the valid condition. Indeed, the median of the perceived depth of the monocular line is behind the minimal depth imposed by the occluder, and as discussed in the section above, the interpretation of the skewness of the perceived depth distribution goes in the same direction. However, in the invalid condition, the monocular line was perceived slightly behind the occluder plane. This result is clearly inconsistent with camouflage and also deviates slightly from Nakayama and Shimojo's observations (1990). We will come back to this interpretation once we have described our simple model below.

As discussed in the introduction, different studies (Gillam, Blackburn, & Cook, 1995; Ono et al., 1992) have suggested that the depth impressions elicited by Nakayama and Shimojo' stimulus (1990) can be explained by double fusion. To address the double fusion explanation, Gillam, Cook, and Blackburn (2003) designed a da Vinci stimulus where the monocular object is a disk that cannot be "double-fused" with the adjacent edge of the occluder.

Because the results of our first experiment are neither consistent with occlusion nor with double fusion, we decided to run a second experiment to study the implication of double fusion in our stimuli.

3. Experiment 2

3.1. Methods

3.1.1. Participants

Four naïve observers (two having participated in Experiment 1) with a normal or corrected-to-normal vision were recruited in the laboratory building. All participants had experience in psychophysical observation and had normal stereo acuity and transparency sensitivity.

3.1.2. Stimulus presentation

The stereograms were presented using the same setup as for Experiment 1.

3.1.3. Stimuli

Stimuli were identical to the ones used in Experiment 1 except that the monocular line was replaced by a monocular disk (radius 0.25°) (see Fig. 6).

Experimental variables were the same as in Experiment 1. The distance between the monocular line and the black square varied randomly between three values (line eccentricity ε: 10, 19 and 28 arcmin). The eye of presentation (left or right) of the monocular line was counterbalanced and the side of presentation (left or right of the square) varied randomly to create four different conditions. The degree of opacity of the black square varied randomly between three values (100%, 30% and 12% opaque but no outline condition).

3.1.4. Procedure

As in Experiment 1, while keeping the nonius lines aligned, participants were asked to evaluate the perceived azimuth (left–right) and depth (front–back) positions of the monocular disk using an adjustment procedure. Each combination of eccentricity values, eye-of-origin, opacity values and validity configurations was repeated 12 times in total. The experiment was divided in 12 short sessions.

3.1.5. Data analysis

Data were averaged for the "side of the disk" factor to bring the total number of trials per condition to 24. As in Experiment 1, data analysis was conducted on the raw coordinates of the stereo-probe (VEA for the Viewing Eye Angle and OEA for the Other Eye Angle).

3.1.6. Predictions

If the results obtained in the first experiment are due at least partly to double fusion then we expect the depth estimations in the second experiment to be different from those the first experiment. If there is no implication of double fusion mechanisms in da Vinci stereopsis (as elicited by our stimuli), we expect the same effects as in the first experiment.

3.2. Results

As for Experiment 1, results are presented as if they resulted from the left eye condition (the disk is presented to the left eye, on the left side of the occluder in the valid condition and on the right side in the invalid condition). The distributions of OEA and VEA reports are shown in Fig. 7.

3.2.1. Main effects of experimental variables

As for Experiment 1, the normality of OEA and VEA distributions was tested using the D'Agostino normality test (D'Agostino, Belanger, & D'Agostino, 1990). Except for three OEA distributions ($\varepsilon = 19$ and 28 for the invalid condition and $\varepsilon = 19$ for the valid condition), all distributions were normal. To take into account the non-normality of a minority of OEA distributions, we conducted a repeated measures ANOVA on the median for each validity condition separately. The ANOVA conducted on the OEA measures revealed a significant effect of eccentricity ($F(2,6) = 8.34$, $P < 0.05$ for the valid condition and $F(2,6) = 0.471$, $P < 0.001$ for the invalid condition) but no effect of opacity ($F(3,9) = 2.68$, $P = 0.110$ for the valid condition and $F(3,9) = 1.733$, $P = 0.230$ for the invalid condition). The ANOVA conducted on the VEA measures revealed the same pattern of results (eccentricity: $F(2,6) = 65.7$, $P < 0.001$ for the valid condition and $F(2,6) = 69.0$, $P < 0.001$ for the invalid condition; opacity: $F(3,9) = 2.23$, $P = 0.154$ for the valid condition and $F(3,9) = 4.89$, $P = 0.028$ for the invalid condition). The ANOVA revealed a significant effect of transparency in the invalid condition. However, this effect was inconsistent across opacity conditions (the perceived horizontal position of the monocular line did not vary with a consistent pattern as opacity decreased).

Because no consistent effect of transparency was found, data were averaged across all opacity conditions for further analyses.

3.2.1.1. Valid condition. The OEA values were significantly smaller than the occlusion predictions for the 10 and 19 arcmin conditions

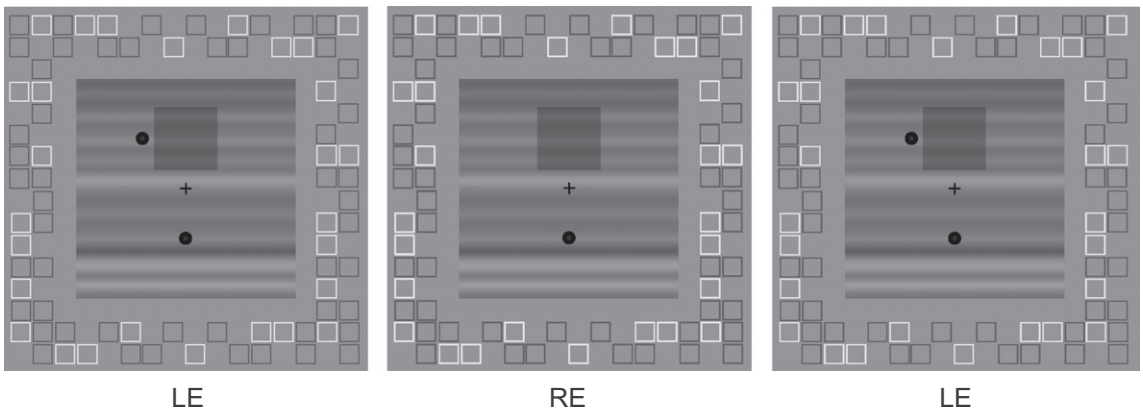

Fig. 6. Stimulus used in Experiment 2 in the 30% opaque condition (the other opacity conditions are not shown). The occlusion or valid condition can be seen by parallel-fusing the first and second columns. The monocular line is replaced by a monocular disk.

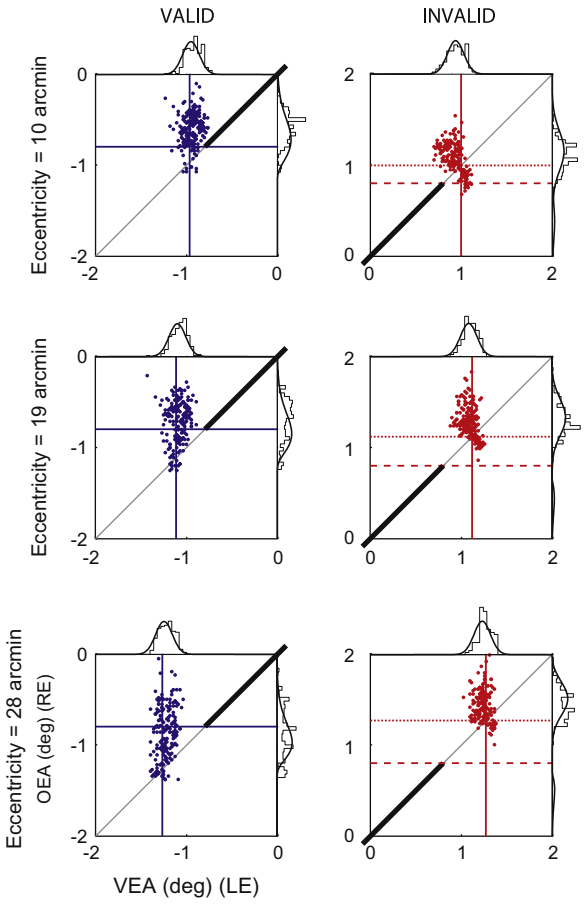

Fig. 7. Results of Experiment 2. See legend from Fig. 4 for details.

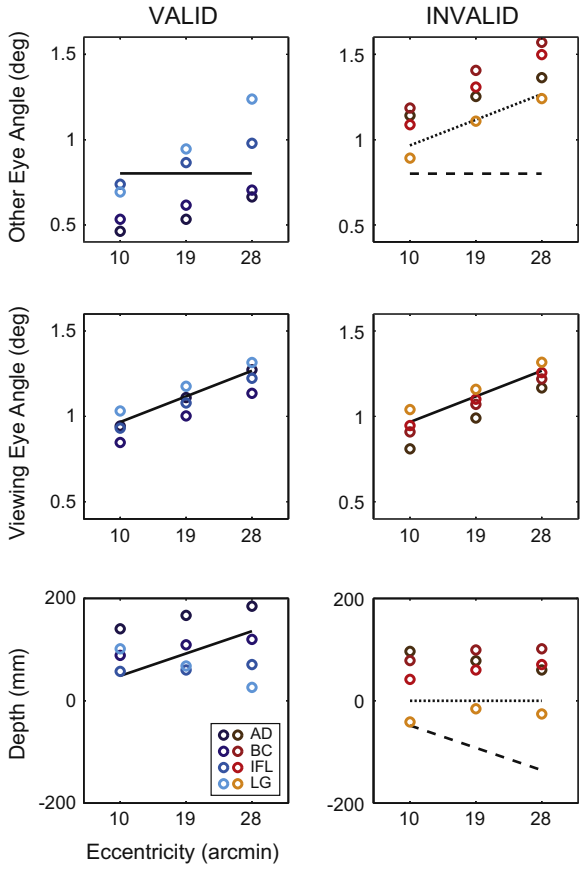

Fig. 8. Individual medians and for Experiment 2. See legend from Fig. 5 for details.

and significantly larger from the prediction for the 28 arcmin condition (CI for ε_{10}: [0.564 0.628], CI for ε_{19}: [0.631 0.717], CI for ε_{28}: [0.816 0.938]; prediction = 0.8). The VEA values were significantly smaller than both occlusion and double fusion predictions for the three eccentricities (CI for ε_{10}: [0.920 0.948], prediction = 0.967; CI for ε_{19}: [1.07 1.10], prediction = 1.12; CI for ε_{28}: [1.22 1.26], prediction = 1.27, meaning that the line was perceived closer to the occluder than the position predicted by the monocular object line of sight.

3.2.1.2. Invalid condition. The OEA values were significantly larger than the occlusion predictions for the three eccentricity values (CI for ε_{10}: [1.03 1.11], prediction = 0.967; CI for ε_{19}: [1.23 1.30], prediction = 1.12; CI for ε_{28}: [1.36 1.46], prediction = 1.27). As in the valid condition, the VEA values were significantly smaller than both occlusion and double fusion predictions for the three eccentricities (CI for ε_{10}: [0.912 0.947], prediction = 0.967; CI for ε_{19}: [1.07 1.10], prediction = 1.12; CI for ε_{28}: [1.22 1.25], prediction = 1.27.

3.2.2. Skewness

3.2.2.1. Other Eye Angle. For both valid and invalid conditions, skewness values were similar to the ones obtained in Experiment 1 but smaller: mean positive skewness for the valid condition (mean skewness = 0.386, ranging from −0.097 to 1.78) and negative skewness for the invalid condition, for all three eccentricities and the four observers (mean skewness = −0.752, ranging from −2.51 to 0.088).

3.2.2.2. Viewing Eye Angle. In the valid condition, the skewness of VEA distributions is close to zero on average (mean skewness = −0.019, ranging from −0.589 to 0.685 across observers). In the invalid condition, the skewness of VEA distributions is small but positive on average (mean skewness 0.068, ranging from −0.574 to 0.623).

3.3. Discussion of Experiment 2

The goal of Experiment 2 was to determine whether the results obtained in Experiment 1 could be (partly) explained by double fusion mechanisms. To do so, we used a monocular element (a disk) that cannot be double-fused with the edge of the occluding object.

The data obtained in this experiment were comparable to those in the first experiment, ruling out an exclusive implication of double fusion mechanisms in our stimuli. The depth and azimuth estimations in Experiment 2 are more spread than in Experiment 1 (compare Fig. 7 with Fig. 4). The greater variability for the VEA can be attributed to the fact that the disk is 2.5 times wider than the line. In contrast, the greater variability for the OEA reflects a larger proportion of estimates near the occlusion depth plane.

The most noticeable difference between the two experiments lies in the OEA measure for the valid condition (see Figs. 5 and 8, first and third rows of plots). In the first experiment, OEA measures followed the prediction patterns for the three eccentricities even though they were significantly larger. In the second experiment, OEA measures follow the prediction patterns as in the first experiment for the 10 and 19 arcmin eccentricities, but the regression observed for the 28 arcmin eccentricity is larger that in the first experiment (the perceived depth is significantly smaller than the prediction). This effect is more salient for one particular observer (shown in light blue and orange in Fig. 8). The difference between the two sets of results might

be explained by an implication of double fusion in some trials in the first experiment. Apart from these differences, both experiments provided similar results. In particular, we found a significant effect of eccentricity on OEA that corresponds to a regression to the occlusion depth plane at the largest eccentricity (28 arcmin). We now attempt to explain the effect of eccentricity on OEA with a simple model.

4. Model

Our purpose here is not to develop a complete and biologically plausible model of da Vinci stereopsis, but rather to provide a descriptive model of our results. The model includes three components that are described in more details in Appendix A. The first component characterizes the constraint provided by the edges of the occluder. This constraint favors matches inside the occluder and discourages matches outside the occluder. It is akin to a double-fusion constraint in that it allows the fusion of the monocular line with the edges of the occluder with the difference that it favors only fusion inside the object. The second component characterizes the constraint that monocular objects tend to be matched behind the object rather than in front. This constraint implements the intuitive idea of an opaque occluder that can hide any other object behind it, but precludes the possibility of camouflage. The third component is a preference for small disparities. This last component is useful to eliminate matches near the far edge of the occluder.

Overall, the combination of these three components represents the plausible locations to solve the correspondence problem when a monocular object is presented. We use the exact same model for valid and invalid conditions, the only difference being where the monocular object is presented. The model is then fitted to marginal distributions of OEA and VEA for both valid and invalid conditions, for the three eccentricities (12 distributions in total). The best fit of the model is shown as a continuous line overlaid to Figs. 3 and 6. The fitted parameters of the model are presented in Appendix A.

The model faithfully reproduces the following aspects of the data:

- in the valid condition, the distributions of OEA are skewed with a long tail extending to large depths,
- in the valid condition, we observe an increase of the spread of OEA with eccentricity,
- in the invalid condition, the distributions of OEA are closer to zero disparity than in the valid condition.

Even though the main characteristics of our data are reproduced by our model, data from Experiment 2 are better accounted for than the ones from the first experiment. For instance, the model displays more regression towards zero disparity in the first experiment than what the experimental data show. This suggests that, in the first experiment, observers may have relied on a double-fusion strategy in some trials. The stimulus in the second experiment was designed to avoid any possibility of double matching. The good match between our model and the results from our second experiment suggests that da Vinci stereopsis can be accounted for by a functional model based on scene geometry constraints, a preference for occlusion over camouflage and a prior for small disparities.

Our model implements two separate constraints for the occluder plane (a preference for occlusion over camouflage) and the fixation plane (a prior for small disparities). Although, these two depth planes were identical in our stimuli, our model makes clear predictions on the perceived position of the monocular object for a change in the occluder's depth.

5. General discussion

5.1. Summary of results from Experiments 1 and 2

We found comparable results in two experiments that used a line and a disk as monocular objects in the vicinity of an occluder. First, there was no effect of transparency on the perceived depth of the monocular object. Second, depth estimations in the valid condition were more consistent with an occlusion explanation than double fusion: the median perceived depth was within the constraint zone and the distribution of depths extended into the constraint zone (at least for small eccentricities). However, depth estimations in the invalid condition were neither in agreement with occlusion nor double fusion: the median depth was behind the occluder's plane (rather than in front) and its distribution spread over a wide range.

5.2. Implications for stereo algorithms processing unpaired features

There are two classes of strategies to infer depth for unpaired features. Monocular regions can be included at the final stages of stereo matching, to refine the disparity map (Jones & Malik, 1992): this map is processed post hoc to determine the likely localizations of depth discontinuities. In this view, occlusion relationships must be derived from the geometry of the scene before they can be integrated into the depth map. Unpaired features thus cannot be used to facilitate the construction of stereoscopic depth.

Another strategy is to postulate that there are early mechanisms capable of detecting monocular regions and occluding contours. In this view, occlusion geometry can serve as a depth cue to constrain the resolution of the matching problem (by excluding unpaired points as matching candidates) and construct the depth map of the scene. Following Nakayama and Shimojo's (1990) study, Anderson and Nakayama (1994) proposed the existence of neurons whose receptive fields are capable of sensing occlusion relationships. These occlusion relationships are extracted by hypothetical mechanisms based on eye-of-origin information and depth discontinuities. In this model, the opacity of the occluding surface is not mentioned as being critical for the processing of half-occlusion configurations. Following Anderson and Nakayama's proposal, several models postulate that the geometry of occlusion is extracted early but they differ in the mechanisms responsible for this computation (Geiger, Ladendorf, & Yuille, 1995; Grossberg & Howe, 2003; Hayashi et al., 2004; Watanabe & Fukushima, 1999). More recently, Assee and Qian (2007) pointed out the fact that these models are not parsimonious and postulate the existence of specific monocular cells. Their model is based on a simple V1–V2 feedforward structure. Depth edges and monocular regions are extracted in V2 from the outputs of V1 binocular cells.

None of the models reviewed above implement the opacity constraint as being dependent on the material properties of the occluding surface. Our results are consistent with this view and suggest that opacity, if critical for the processing of half-occlusions, is not extracted on the basis of transmittance. In this case, the opacity constraint might be achieved by implementing a simple uniqueness rule (each item from each image must be assigned at most one disparity value), as proposed by Watanabe and Fukushima (1999). This algorithm is based on the constraint that an occluding point should always exist between an unpaired point and the eye that cannot see the unpaired point.

Aside from the computational models described in this section, we propose a functional model based on the geometrical constraints of the visual scene, a bias toward occlusion rather than camouflage and a prior for small disparities. These components

can be implemented at a mid-level stage of visual processing. In this view, a general preference for small disparities is combined with the scene geometry to constrain the disparity map.

6. Conclusion

In conclusion, we failed at demonstrating that there is an interaction between perceptual transparency and da Vinci stereopsis. These results suggest that da Vinci stereopsis is solved during relatively early stages of stereoscopic processing but at the same time that it is constrained by basic geometrical information in the visual scene. By looking at the full distributions of depth and azimuth estimations rather than simply the means, we were able to describe more meticulously the percepts evoked by da Vinci stereopsis. Overall, our study questions the traditional view of stereopsis that is primarily concerned by the resolution of the correspondence problem and neglects the scene geometry.

Acknowledgments

We thank Laurie Wilcox for discussions and Michael Landy and two reviewers for their comments on an earlier draft of this manuscript. This work was supported by a Grant from the French Ministère de l'Enseignement Supérieur et de la Recherche, and by Grant ANR-2010-BLAN-1910-01 from the French Agence Nationale de la Recherche.

Appendix A

We describe here in more details the model used to determine the distributions of perceived locations of the monocular object. The model attempts to reveal all the possible locations where a monocular object could be in agreement with the occluder. In other words, we are interested in estimating the conditional probability

$$p(\mathrm{LEA}, \mathrm{REA}|\mathrm{occluder}) \tag{1}$$

where (LEA, REA) represent the coordinates (left and right eye angles) of any monocular object that can be perceived in the vicinity of the occluder. In a traditional Bayesian way, this posterior conditional distribution can be re-written as the product of a likelihood provided by the occluder and a prior expectation on the location of the monocular object (Mamassian, Landy, & Maloney, 2002)

$$p(\mathrm{LEA}, \mathrm{REA}|\mathrm{occluder}) \propto p(\mathrm{occluder}|\mathrm{LEA}, \mathrm{REA})p(\mathrm{LEA}, \mathrm{REA}) \tag{2}$$

The first term on the right-hand side of Eq. (2) represents the constraint imposed by the occluder. We assume it is the combination of two components. The first component corresponds to the constraint provided by the edges. If ω is the half-width of the occluder, then this constraint for the left eye angle (LEA) can be written

$$C_1(\mathrm{LEA}) = \left(\frac{\mathrm{LEA}-\omega}{\sigma_1^2}\right)\exp\left(-\frac{(\mathrm{LEA}-\omega)^2}{2\sigma_1^2}\right) - \left(\frac{\mathrm{LEA}+\omega}{\sigma_1^2}\right)\exp\left(-\frac{(\mathrm{LEA}+\omega)^2}{2\sigma_1^2}\right) \tag{3}$$

where σ_1^2 represents the spatial uncertainty on the edge constraint. This constraint has two parts corresponding to the left and right edges of the occluder. A similar expression applies to the right eye angle $C_1(\mathrm{REA})$.

The second component of the model favors hidden objects placed behind the occluder. It represents an opacity constraint and can be written as

$$C_2(\mathrm{LEA}, \mathrm{REA}) = -\left(\frac{\mathrm{LEA}-\mathrm{REA}}{\sigma_2^2}\right)\exp\left(-\frac{(\mathrm{LEA}-\mathrm{REA})^2}{2\sigma_2^2}\right) \tag{4}$$

where σ_2^2 represents the spatial uncertainty on the opacity constraint. The edge and opacity constraints combine to provide an overall constraint provided by the occluder. We take this combination to be a weighted sum where a weight α is assigned to the opacity constraint. The overall constraint provided by the occluder is therefore

$$p(\mathrm{occluder}|\mathrm{LEA}, \mathrm{REA}) \propto \lfloor C_1(\mathrm{LEA}) + C_1(\mathrm{REA}) + \alpha C_2(\mathrm{LEA}, \mathrm{REA}) \rfloor \tag{5}$$

where the symbols $\lfloor\rfloor$ indicate that we take only the positive part of this combination.

The third component of the model is a prior for small disparities

$$p(\mathrm{LEA}, \mathrm{REA}) \propto \exp\left(-\frac{(\mathrm{LEA}-\mathrm{REA})^2}{2\sigma_3^2}\right) \tag{6}$$

where σ_3^2 characterizes the strength of the zero disparity constraint. This prior constraint is combined with the overall occluder constraint (Eq. (5)) according to Eq. (2). The proportional sign in that equation corresponds to the fact that the product has to be normalized so that the posterior is a probability distribution (*i.e.* sums to 1; see Mamassian, Landy, & Maloney, 2002).

All together, the occluder constraint and the prior for small disparities define the locations in binocular space where a monocular object can be seen in the vicinity of the occluder. We have represented these locations in Fig. 9, where for the purpose of the illustration, we have preserved the negative parts of the occluder computation in Eq. (5). We note that the areas where a monocular line can easily be matched (in orange) are behind the occluder, as well as slightly to the left of the occluder for the left eye and slightly to the right for the right eye. In contrast, there are two inhibitory zones (in blue) on either side of the occluder. These inhibitory zones are responsible for the skewness of the distribution of reported depth of the monocular objects in our data.

To obtain quantitative predictions for the monocular line or disk stimuli, we assume that these stimuli are located with their own uncertainty

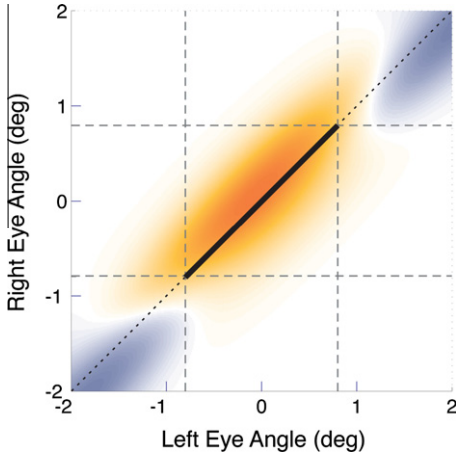

Fig. 9. Modeled constrained space by the occluder. The occluder is shown as a thick black diagonal line between −0.8° and +0.8° in both eyes, thus perceived as a fronto-parallel rectangle of width 1.6°. The model attempts to reveal the locations in binocular space where an object presented monocularly could be perceived in agreement with the occluder. Orange locations indicate positive areas, namely locations where a monocular object could indeed be matched. Blue locations indicate negative areas, namely locations where correspondence would be inhibited. See Appendix A for model details.

Table 1
Parameters of the model adjusted to the experimental results.

	σ_1 (deg)	σ_2 (deg)	α	σ_3 (deg)	σ_4 (deg)
Experiment 1 (line)	1.06	0.35	0.42	0.33	0.051
Experiment 2 (disk)	1.12	0.24	0.49	0.36	0.093

$$M(\mathrm{VEA}) = \exp\left(-\frac{(\mathrm{VEA} - (\omega + \varepsilon))^2}{2\sigma_4^2}\right) \quad (7)$$

where $(\omega + \varepsilon)$ is the physical location of the monocular object (when it is left of the occluder) and σ_4^2 characterizes its spatial uncertainty. This latter parameter can be adjusted to take into account the width of the monocular object (a wider object – e.g. a disk compared to a line – carries more spatial uncertainty). This monocular object constraint is combined with the posterior distribution by taking their product. In the end, we obtain as a model

$$p(\mathrm{VEA}, \mathrm{OEA}) \propto p(\mathrm{VEA}, \mathrm{OEA}|\mathrm{occluder})M(\mathrm{VEA}) \quad (8)$$

where the proportional sign is again used here to guarantee a probability distribution function for possible pairs of VEA and OEA associated to a specific monocular object.

The exact same model is used for valid and invalid conditions, the only difference being the location of the monocular object. From the model, we extract the distributions of VEA and OEA for each of the six experimental conditions (valid and invalid locations of the monocular object for the three eccentricities). We then adjust the five parameters of the model to minimize the squared distance between the predicted distributions and the data. The fitted parameters of the model are presented in Table 1 and the best fitted distributions are superimposed onto Figs. 4 and 7.

References

Anderson, B. L. (2008). Transparency and occlusion. In A. I. Basbaum, A. Kaneko, G. M. Shepherd, & G. Westheimer (Eds.) & T. D. Albright & R. Masland (Vol. Eds.), *The senses: A comprehensive reference* (Vol. 2, Vision II, pp. 239–244). San Diego: Academic Press.

Anderson, B., & Nakayama, K. (1994). Toward a general theory of stereopsis: Binocular matching, occluding contours, and fusion. *Psychological Review, 101*(3), 414–445.

Assee, A., & Qian, N. (2007). Solving da Vinci stereopsis with depth-edge-selective V2 cells. *Vision Research, 47*(20), 2585–2602.

Backus, B. T., Fleet, D. J., Parker, A. J., & Heeger, D. J. (2001). Human cortical activity correlates with stereoscopic depth perception. *Journal of Neurophysiology, 86*, 2054–2068.

Brainard, D. (1997). The psychophysics toolbox. *Spatial Vision, 10*(4), 433–436.

Cook, M., & Gillam, B. (2004). Depth of monocular elements in a binocular scene: The conditions for da Vinci stereopsis. *Journal of Experimental Psychology: Human Perception and Performance, 30*(1), 92–103.

D'Agostino, R. B., Belanger, A., & D'Agostino, R. B. J. (1990). A suggestion for using powerful and informative tests of normality. *The American Statistician, 44*(4), 31–321.

Efron, B., & Tibshirani, R. J. (1994). *An introduction to the bootstrap*. New York: Chapman & Hall.

Geiger, D., Ladendorf, B., & Yuille, A. (1995). Occlusions and binocular stereo. *International Journal of Computer Vision, 14*, 211–226.

Gillam, B., Blackburn, S., & Cook, M. (1995). Panum's limiting case: Double fusion, convergence error, or 'da Vinci stereopsis'. *Perception, 24*(3), 333–346.

Gillam, B., & Borsting, E. (1988). The role of monocular regions in stereoscopic displays. *Perception, 17*, 603–608.

Gillam, B., Cook, M., & Blackburn, S. (2003). Monocular discs in the occlusion zones of binocular surfaces do not have quantitative depth – A comparison with Panum's limiting case. *Perception, 32*(8), 1009–1019.

Grossberg, S., & Howe, P. (2003). A laminar cortical model of stereopsis and three-dimensional surface perception. *Vision Research, 43*(7), 801–829.

Häkkinen, J., & Nyman, G. (1996). Depth asymmetry in da Vinci stereopsis. *Vision Research, 36*(23), 3815–3819.

Harris, J. M., & Wilcox, L. M. (2009). The role of monocularly visible regions in depth and surface perception. *Vision Research, 49*, 2666–2685.

Hayashi, R., Maeda, T., Shimojo, S., & Tachi, S. (2004). An integrative model of binocular vision: A stereo model utilizing interocularly unpaired points produces both depth and binocular rivalry. *Vision Research, 44*(20), 2367–2380.

Howard, I. P., & Rogers, B. J. (2002). *Seeing in depth* (Vol. II). Porteous Press.

Hubel, D. H., & Wiesel, T. N. (1959). Receptive fields of single neurons in the cat's striate cortex. *Journal of Physiology, 148*, 574–591.

Jones, J., & Malik, J. (1992). *A computational framework for determining stereo correspondence from a set of linear spatial filters*. Berkeley: University of California, Computer Science Division (EECS).

Lawson, R., & Gulick, W. (1967). Stereopsis and anomalous contour. *Vision Research, 7*(3), 271–297.

Mamassian, P., Landy, M. S., & Maloney, L. T. (2002). Bayesian modelling of visual perception. In R. Rao, B. Olshausen, & M. Lewicki (Eds.), *Probabilistic models of the brain: Perception and neural function* (pp. 13–36). Cambridge, MA: MIT Press.

Metelli, F. (1985). Stimulation and perception of transparency. *Psychological Research, 47*(4), 185–202.

Nakayama, K., & Shimojo, S. (1990). Da Vinci stereopsis: Depth and subjective occluding contours from unpaired image points. *Vision Research, 30*(11), 1811–1825.

Ono, H., Shimono, K., & Shibuta, K. (1992). Occlusion as a depth cue in the Wheatstone–Panum limiting case. *Perception and Psychophysics, 51*(1), 3–13.

Panum, P. L. (1858). Untersuchungen uber das Sehen mit Zwei Augen. *Kiel*.

Parker, A. J. (2007). Binocular depth perception and the cerebral cortex. *Nature Review Neuroscience, 8*(5), 379–391.

Pelli, D. (1997). The VideoToolbox software for visual psychophysics: Transforming numbers into movies. *Spatial Vision, 10*(4), 437–442.

Pianta, M., & Gillam, B. (2003). Paired and unpaired features can be equally effective in human depth perception. *Vision Research, 43*(1), 1–6.

Porter, T., & Duff, T. (1984). Compositing digital images. *Computer Graphics, 18*(3), 253–259.

Preston, T. P., Li, S., Kourtzi, Z., & Welchman, A. E. (2008). FMRI selectivity for perceptually-relevant binocular disparities in the human brain. *Journal of Neuroscience, 28*, 11315–11327.

Qiu, F., & Von Der Heydt, R. (2007). Neural representation of transparent overlay. *Nature Neuroscience, 10*(3), 283–284.

Sekuler, A. B., & Palmer, S. E. (1992). Perception of partly occluded objects: A microgenetic analysis. *Journal of Experimental Psychology: General, 121*(1), 95–111.

Singh, M., & Anderson, B. (2002). Toward a perceptual theory of transparency. *Psychological Review, 109*(3), 492–519.

Watanabe, O., & Fukushima, K. (1999). Stereo algorithm that extracts a depth cue from interocularly unpaired points. *Neural networks: The official journal of the International Neural Network Society, 12*(4–5), 569–578.